ISSN (Print) : 2320 – 3765
ISSN (Online): 2278 – 8875

International Journal of Advanced Research in Electrical, Electronics and Instrumentation Engineering

(An ISO 3297: 2007 Certified Organization)

Vol. 4, Issue 1, January 2015

Elastic Registration of Cardiac Images Using Automatic Segmentation

E. Suresh[1] , Ms.R.Renita Rexy*[2,] Dr. K.V.S.S.S.S.Sairam

Assistant Professor, Dept. of ECE, Jerusalem College of Engineering, Chennai, Tamil Nadu, India[1]

Assistant Professor, Dept. of ECE, Bharath University, Chennai, Tamil Nadu, India[2]

Associate Professor, Dept. of ECE, Bharath University, Chennai, Tamil Nadu, India[3]

* Corresponding Author

ABSTRACT: in this paper, we propose a automatic segmentation method that uses saliency and gradient information for registration of dynamic contrast enhanced (DCE) magnetic resonance (MR) images of the heart. DCE-MR images are characterized by rapid intensity changes over time, thus posing challenges for conventional intensity-based registration methods. Saliency information contributes to a contrast invariant metric to identify similar regions in spite of contrast enhancement. Its robustness and accuracy are attributed to a close adherence to a neurobiological model of the human visual system (HVS). This ability motivated us to explore the efficacy of such a model for registering DCE-MR images. The data penalty is a combination of saliency and gradient information. The smoothness cost depends upon the relative displacement and saliency difference of neighboring pixels.

KEYWORDS: Contrast-invariant, elastic registration, magnetic resonance (MR) images, Markov random fields (MRFs), saliency.

I. INTRODUCTION

REGISTRATION is one of the fundamental problems in image processing and is important for many applications such as medical image analysis, building prior models from training images, and segmentation of image sequences. Registration is of two types: rigid and non rigid registration. Non rigid registration for correcting elastic deformation of organs is a very important preliminary step for automated or semi automated medical image analysis. Over the years, many methods have been proposed to meet the challenges of registering elastic deformations in images. A detailed review on the principles of non rigid image registration can be found in [1] and [2]. By designing appropriate cost functions, existing elastic registration frameworks have successfully registered a wide variety of images. Popular techniques include elastic models [3], fluid flow methods [4], [5], optical flow-based methods [6], thin plate splines [7], freeform deformations (*FFD*) using B-splines [8], [9], and radial basis functions [10]. Mutual information-based methods have been used for non rigid registration in [8] and [11].

Recently, Markov random fields (MRFs) were used for elastic registration of natural and medical images by formulating it as a discrete labeling problem [12]–[14]. Shekhovtsov *et al.* in [12] use pixel blocks in formulating the MRF energy function to compensate for non rigid deformations in synthetic and real images. Smoothness was imposed based on the relative displacement between neighboring pixels. Tang and Chung in [15] use MRFs to register brain images and impose smoothness using first derivatives. In [13], Glocker *et al.* introduce a novel approach for dense image registration. The objective function is defined using MRFs and the dense deformation field is defined using a registration grid with interpolation, thus allowing for dimensionality reduction. Mahapatra and Sun in [14] use saliency information to identify corresponding regions in a pair of pre- and post contrast enhanced kidney perfusion images and elastically register those using MRFs.

Majority of the non rigid registration algorithms are purely intensity based and do not give satisfactory results in the presence of intensity changes. Dynamic contrast enhanced (DCE) magnetic resonance imaging (MRI) is a popular technique used for the functional analysis of internal organs. A contrast agent is injected intravenously into the patient and a sequence of MR images obtained over a period of time. The flow of contrast agent leads to large intensity

ISSN (Print) : 2320 – 3765
ISSN (Online): 2278 – 8875

International Journal of Advanced Research in Electrical, Electronics and Instrumentation Engineering

(An ISO 3297: 2007 Certified Organization)

Vol. 4, Issue 1, January 2015

changes over a short time period and highlights various cardiac tissues. By monitoring this intensity variation, radiologists perform a functional analysis of the heart to facilitate diagnosis and early identification of cardiovascular diseases. This requires a similarity metric to deal with intensity change. Visual saliency, which is a measure of how different a region is from its surroundings, provides useful information to establish correspondence between pre- and post contrast images [14].

A. Saliency-Based Registration

Salient regions or points are prominent in a scene or image. Thus, it is natural that these salient landmarks influence the task in hand, e.g., registration. Previous works have used salient landmarks and regions for registration and matching [16]–[18]. Ou *et al.* in [16] use Gabor attributes at each voxel to identify salient structures. They do not exclusively define saliency as a metric but use the concept of "mutual saliency" that measures the uniqueness of correspondence between two landmarks and assigns weights for the purpose of registration. Use of Gabor coefficients makes the method computationally expensive involving numerous calculations in selecting the right attributes. Other works, [17], identify salient regions using entropy-based scale-invariant region features defined in [18]. The entropy based saliency model (or scale-space maps) of [18] is sensitive to noise. Further, any change in intensity (as in perfusion images) alters the entropy measure of a neighborhood leading to different saliency measures for the same voxel. The neurobiology-based saliency model of [19] has the following advantages over scale space maps [20]: 1) less sensitive to noise and intensity change; 2) lower computation time; and 3) close agreement with human fixations [21].

Our study uses visual saliency information in MRFs for non rigid registration of dynamic MR images of the heart. It can effectively correct elastic deformations in the presence of intensity change due to flow of contrast agent. The contribution of this paper is twofold. First, we introduce a modified neurobiological saliency model that determines saliency information based on local information. This is suitable for elastic registration where matching local similarity features is important. It is different from [14] where the saliency model gave a global map, making the procedure sensitive to large deformations. Second, we achieve registration using a combination of gradient and saliency information because intensity information can be misleading for contrast enhanced images. The use of saliency maps is inspired by the working of the human visual system (HVS). Humans have a remarkable capability to match images or objects in the presence of noise or intensity change. Therefore, we have explored a computational model of the HVS in registration tasks. It proves to be robust and identifies similar pixels in spite of contrast enhancement. Edge orientation information complements saliency information in the registration process. The description of our modified saliency model, which is based on principles of neurobiology, is given in Section II. In Section III, we describe the use of saliency and edge orientation information for elastic registration using MRFs. Subsequently, we show results for real patient cardiac and liver datasets in Section IV and report our conclusion in Section V.

II. SALIENCY MODEL

Saliency defines the degree to which a particular region is different from its neighbors about certain features such as intensity, edge orientation, color, etc. It is based on a biologically plausible architecture proposed in [22]. Visual input is first decomposed into a set of topographic feature maps and different spatial locations compete for saliency within each map, such that only locations that stand out from their neighbors are highlighted. These feature maps are then combined to form a final saliency map that highlights the most salient regions in an image.

The original model by Itti-Koch [19] gives a saliency measure that is more suited for global registration tasks like rigid registration [20]. Elastic registration aims to match pixels based on local neighborhood information. For the saliency maps to reflect the local information, we modify the original model by using a local neighborhood of a pixel instead of a Gaussian pyramid to determine a pixel's saliency. Feature maps corresponding to intensity and edge information are computed for each image. Let $F(s)$ denote the feature value at pixel s in feature map F. The neighborhood of s is denoted by N_s. According to neurobiological studies, the field of view of the eye's fovea covers an area of 1◦ [23], i.e., when we look at a point, information from a neighborhood of 1◦ is also processed. An area of 1◦ is equivalent to a pixel neighborhood of size 21 × 21 [23]. The response function of cortical cells is a Gaussian function, i.e., further away a point less is its influence on the central pixel. Thus, to calculate how different a pixel is from its surroundings with respect to a certain feature, a sum of weighted difference of feature values is calculated, i.e.,

ISSN (Print) : 2320 – 3765
ISSN (Online): 2278 – 8875

International Journal of Advanced Research in Electrical, Electronics and Instrumentation Engineering

(An ISO 3297: 2007 Certified Organization)

Vol. 4, Issue 1, January 2015

$$D_F(s) = \sum_i \exp(-\| s - s_i \|) | F(S) - F(S_i) | \quad (1)$$

where D_F indicates the difference map for feature F; s_i is the i^{th} pixel in the 21 × 21 neighborhood of pixel s; $\|s - s_i\|$ denotes the Euclidean distance between s and s_i . $F(s_i)$ denotes the feature value at pixel si .

The difference maps represent different modalities and varying extraction mechanisms. Before combining them, we normalize the maps so that salient objects appearing strongly in a few maps are not masked by noise or less salient objects present in other maps. A map normalization operator, $N(.)$, comprising the following steps is used.

1) Normalize the values in the map to a fixed range $(0 \cdots M)$ to eliminate modality- or feature-dependent amplitude differences. We set $M = 1$ for all feature maps in our experiments.

2) Find the location of the map's global maxima M and Calculate $\overline{m}$, the average of its other local maxima.

3) Globally multiply the map by $(M - \overline{m})^2$. The biological motivation behind $N(.)$ is the coarse replication of lateral inhibition mechanisms where neighboring similar features inhibit each other via specific, anatomically defined connections[24]. The two difference maps, D_I for intensity and D_O for edge orientation, are normalized, and the final saliency map Γ is the weighted average given by

$$\Gamma = w_1 N(D_I) + (1 - w_1) N(Do) \quad . (2)$$

W1 is a weight that determines the relative contribution of each feature to the final map. Edge information being a more robust metric for matching pixels in a pair of contrast enhanced images is given greater importance (i.e., w_1 = 0.3). The importance of a neurobiology-based visual saliency model on a registration task can be accessed from the fact that landmark points are those determined by the user to convey important information for registration. The choice of landmarks is a natural result of their visual importance in terms of intensity and edge orientations.

Fig. 1 shows images from different stages of contrast enhancement (first row) along with the saliency maps obtained using our modified saliency model (second row) and the original model of [19] (third row). Fig. 1(a) shows the reference image for a dataset and Fig. 1(b)–(d) shows the floating images corresponding to different stages of contrast enhancement. Their respective saliency maps using our modified model are shown in Fig. 1(e)–(h). They are very similar to each other in spite of the intensity change due to contrast enhancement, and also capture the fine structures and other landmarks in the actual image. Although there are minor differences in the saliency map, it is able to capture the change in shape of the left ventricle (LV) due to deformations.

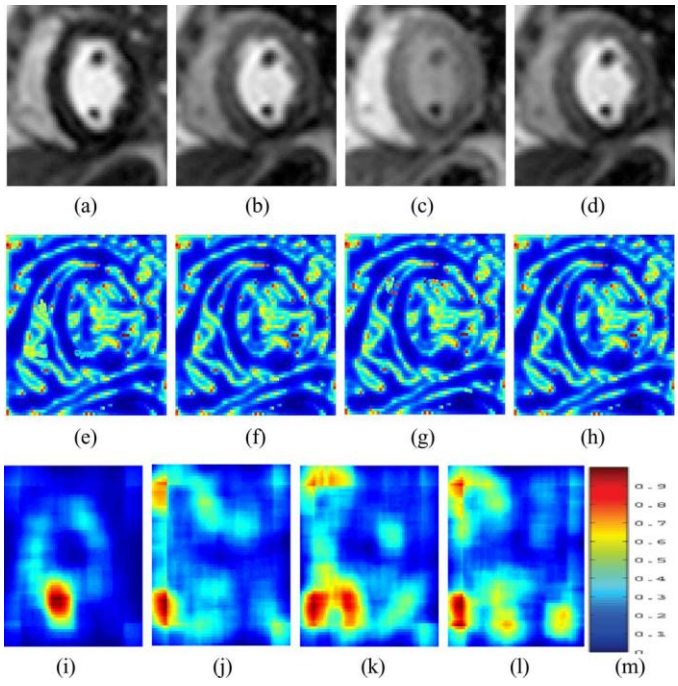

ISSN (Print) : 2320 – 3765
ISSN (Online): 2278 – 8875

International Journal of Advanced Research in Electrical, Electronics and Instrumentation Engineering

(An ISO 3297: 2007 Certified Organization)

Vol. 4, Issue 1, January 2015

Fig. 1. Saliency maps of contrast enhanced image sequence. Cardiac images from different stages of contrast enhancement are shown: (a) target frame, (b)– (d) images from different stages of contrast enhancement. (e)–(h) Respective saliency maps from our modified saliency model. The saliency maps are seen to be similar; (i)–(l) saliency maps obtained using the original model in [19]; the saliency maps are sparse and exhibit lot of variability. (m) Color bar for the saliency maps. Color images are for illustration purposes.

A. Saliency Maps for Cardiac MRI

This is in stark contrast to the saliency maps of the original model of [19] [Fig. 1(i)–(l)]. Those maps do not provide information on the finer structure of the cardiac muscles which is essential for elastic registration. They are sparse and do not reflect the change in shape of the LV. Thus, our modified saliency model allows us to match different regions for similarity in spite of contrast enhancement.

B. Limitations of Saliency

Saliency is not always a perfect contrast invariant feature, and may occasionally assign different saliency values to corresponding pixels in a pair of contrast enhanced images. In Fig. 1(g), the saliency values at the upper edge of the LV are not the same as in Fig. 1(e), (f), and (h). The use of intensity information in (2) may play a role in the limitations of saliency-based registration. The changing intensity could influence the saliency maps, especially for perfusion images. Although gradient orientation information acts as a more robust contrast invariant metric, the contribution of intensity toward saliency cannot be completely ruled out. Psychophysical studies in [23] clearly establish the importance of both intensity and edge information in determining saliency. As a result, we give greater importance to gradient orientation information when calculating saliency maps. Thus, we may infer that intensity information could have a role in the limitations of saliency for registration. Another common characteristic observed in perfusion MRI is the change in intensity of the background due to artifacts arising from image acquisition. This may lead to different saliency maps for images from similar stages of contrast enhancement. Although this is not observed very frequently, it can lead to misregistration between images.

III. METHOD

A. Saliency-Based Registration

The goal of registration is to match each pixel in the floating image to the most similar pixel in the reference image, and the feature depends on the type of images being registered. MRFs are used for discrete labeling problems and a smooth solution is obtained by constraining the relative displacement between neighboring pixels to be within a specified range, so that they have similar displacement labels. A combination of gradient and saliency information is used to register DCE images because intensity information can be misleading for registering contrast enhanced images.

B. Markov Random Fields

The energy function of an MRF takes the following form:

$$E(x) = \sum_{s \in P} Ds(x_s) + \sum_{(s,t) \in N} Vst(x_s, x_t) \qquad (3)$$

Where P denotes the set of pixels x_s denotes the label of pixel $s \in P$; N is the set of neighboring pixel pairs. $x_s = \{x_s^1 + x_s^2\}$ denotes the displacements along the two axes. The labels of the entire set of pixels are denoted by x. Ds is a unary data penalty function derived from observed data that measures how well label x_s fits pixel s, Vst and is a pair wise interaction potential used to impose smoothness and measures the cost of assigning labels x_s and x_t to neighboring pixels s and t.

ISSN (Print) : 2320 – 3765
ISSN (Online): 2278 – 8875

International Journal of Advanced Research in Electrical, Electronics and Instrumentation Engineering

(An ISO 3297: 2007 Certified Organization)

Vol. 4, Issue 1, January 2015

1) Data Penalty Term: Ds assigns a penalty to a pixel *s* taking on a particular label x_s .We define *Ds* as a combination of saliency and gradient information. We refer to the block centered at pixel *s* in an image as block *s*. A pixel block is used to calculate the data penalty value for greater accuracy and robustness. *Ds* is given by

$$Ds(x_s) = \frac{1}{2}\left[1 - \bar{w}(x_s, s) \times \overline{\cos}(x_s, s)\right] \qquad (3)$$

$\bar{w}(x_s, s)$ is a function of saliency information and $\overline{\cos}(x_s, s)$ is a function of edge information. $\overline{\cos}(x_s, s)$ is a normalized metric depending on edge magnitudes and orientation angles of the pair of pixels.

2) Pairwise Interaction Term: Being the interaction term between the pixel and its neighbors, $Vst(x_s, x_t)$ plays an important role in ensuring continuity or smoothness in the registration framework. We define it as

$$Vst = \begin{cases} 0.002, |x_s - x_t| \le \sqrt{2} and \left|\Gamma s - \Gamma t\right| \le 0.4 \\ 0.002, |x_s - x_t| \le 3 and \left|\Gamma s - \Gamma t\right| > 0.4 \\ \infty, otherwise \end{cases} \qquad (4)$$

C. Optimization Using Modified Narrow Band Graph Cuts

Pixels are represented as nodes *V p* in a graph *G* which also consists of a set of directed edges *E* that connect two nodes. The edge weight between two neighboring nodes is the smoothness term while the data penalty term is the edge weight for links between nodes and label nodes (terminal nodes). The optimum labeling set is obtained by severing the edge links in such a manner that the cost of the cut is minimum. The number of nodes is equal to the number of pixels *N p* and the number of labels is equal to *L*. For every node, the data penalty term is determined as a function of the corresponding floating image and the reference image. Details of graph construction and optimization can be found in [26]. Note that although each pixel is a node in the graph, the data penalty is derived from a block of neighborhood pixels for robustness. Narrow band graph cuts (NBGC) are used to increase the optimization speed of an MRF energy function [27]. An initial solution is obtained for a coarse resolution image. It is propagated to higher resolutions where the candidate solutions are confined to a narrow band. The objective is to reduce the computation time by decreasing the number of nodes in the graph. This can be achieved when there is a reliable way to determine which pixels are important for optimization and which are not.

D. Calculation of Registration Error

A quantitative evaluation of registration accuracy is necessary to judge the effectiveness of any algorithm. The results of registration are generally compared with reference (or ground truth) parameters that help us determine the accuracy of the algorithm. However, it is difficult to get ground truth parameters for elastic registration because each pixel may have different displacement vectors. A common approach is to simulate deformations of known magnitudes and use the magnitude of recovered parameters to calculate the error. Simulated deformations may not replicate deformations found in real-world data. Moreover, simulated deformations could be biased (either favorably or unfavorably) toward certain registration frameworks.

Observations about our algorithm. 1) Since our saliency map is based on the principles of neurobiology, it is a robust similarity metric in the face of contrast enhancement and noise. In combination with gradient information, it increases registration accuracy.

2) Saliency in smoothness formulation adds to the method's robustness. Saliency being more reliable than edge magnitude is more effective to determine whether neighboring pixels in *If* belong to the same object or not.

3) Saliency information helps in reducing computation with the identification of pixels relevant for registration (less than 50% of original number). A coarse-to-fine approach reduces the number of labels and hence, the computation time.

ISSN (Print) : 2320 – 3765
ISSN (Online): 2278 – 8875

International Journal of Advanced Research in Electrical, Electronics and Instrumentation Engineering

(An ISO 3297: 2007 Certified Organization)

Vol. 4, Issue 1, January 2015

Algorithm 1. Registration Framework

Require: I_r, I_f

1: Calculate saliency maps of I_r and I_f.
2: For every pixel s in I_f and all labels calculate the data penalty as a function of saliency and gradient information (Eqn. (4)).
3: Calculate smoothness based on registration labels and saliency information (Eqn. (8)).
4: Identify important nodes (pixels) in the graph using saliency information for implementing SNBGC.
5: Minimize energy function using multi level graph cuts
- determine a coarse displacement labels at spacing of 3 pixels (block size of 11×11).
- determine finer displacement labels at spacing of 1 pixels (block size of 5×5).
- determine sub-pixel displacement at spacing of $1/2$ pixels (block size of 5×5).

6: From the final labels transform I_f to get registered image.

IV. EXPERIMENTS AND RESULTS

A. Cardiac Perfusion MRI

Cardiac images were acquired on Siemens Sonata MR Scanners following bolus injection of Gd-DTPA contrast agent. The image dimensions varied from $(60 - 71) \times (75 - 83)$ with the pixel spacing equivalent to 1.5 mm. The entire scan consists of 60 frames for each dataset. Contrast agent flows into the right ventricle, then into the LV, and finally into the myocardium. The acquired datasets were all in 2-D and a total of 12 datasets were used to test our method. Our approach to determine the

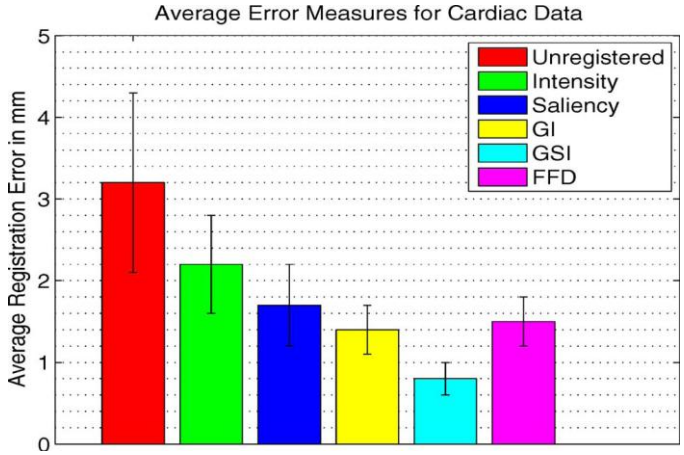

Fig. 2. Average Err values for all 12 cardiac datasets before and after registration.

Results for *Int*, *Sal*, *GI*, and *GSI* are shown. registration error is outlined in Section III-D. We evaluate registration performance based on the following criteria: normalized mutual information (*NMI*), Woods criteria (*WC*) for multimodal images in [28], and average registration error of pixels (*Err*). For each of the aforesaid criteria, we use MRFs with the following similarity measures: sum-of-squared differences using intensity (*Int*), sum-of-squared differences using saliency (*Sal*), gradient information (*GI*) i.e., $w(xs, s) = 1$ in (4), and a combination of gradient and

ISSN (Print) : 2320 – 3765
ISSN (Online): 2278 – 8875

International Journal of Advanced Research in Electrical, Electronics and Instrumentation Engineering

(An ISO 3297: 2007 Certified Organization)

Vol. 4, Issue 1, January 2015

saliency information (*GSI*). Additionally, we also compare the performance of *NMI*-based *FFD* method of [8]. The method is referred to as *FFD*.

Fig. 3 shows results for a typical cardiac dataset where saliency information leads to more accurate registration. After registration is complete, we use the deformation field obtained from each floating image to deform its LV contour so as to match the LV in the reference image. This deformed contour is then overlaid on the corresponding floating image and is shown in red for rows 1–4 of Fig. 3. Columns (1)–(3) denote the images in the first four rows. Each column shows a different floating image corresponding to different stages of contrast enhancement, and each row shows results for different similarity metrics. The reference image for this dataset is shown in Fig. 3(a). The outline of the LV in the reference image is shown in blue for rows 1–4. This gives an idea of the degree of deformation in each floating image, the extent of deformations that can be recovered using each method, and most importantly, the accuracy of each method. For an ideal registration, the red contour and blue contour should completely overlap and any gap between the two contours indicates registration error. The first row shows results for *GSI* followed by results of *GI*, *Int*, and *Sal*. The best registration is achieved for *GSI* as is evident from the minimal gap between the red and blue contours.

Int shows the worst performance because of its exclusive dependence on intensity information. This is observed especially in the first and third images of the third row. Because of its ability to match corresponding regions in contrast enhanced images (see Fig. 1), *Sal* performs better than *Int*. However, its performance degrades with increasing noise levels. *GI* performance is more or less the same as *Sal*. A close observation shows

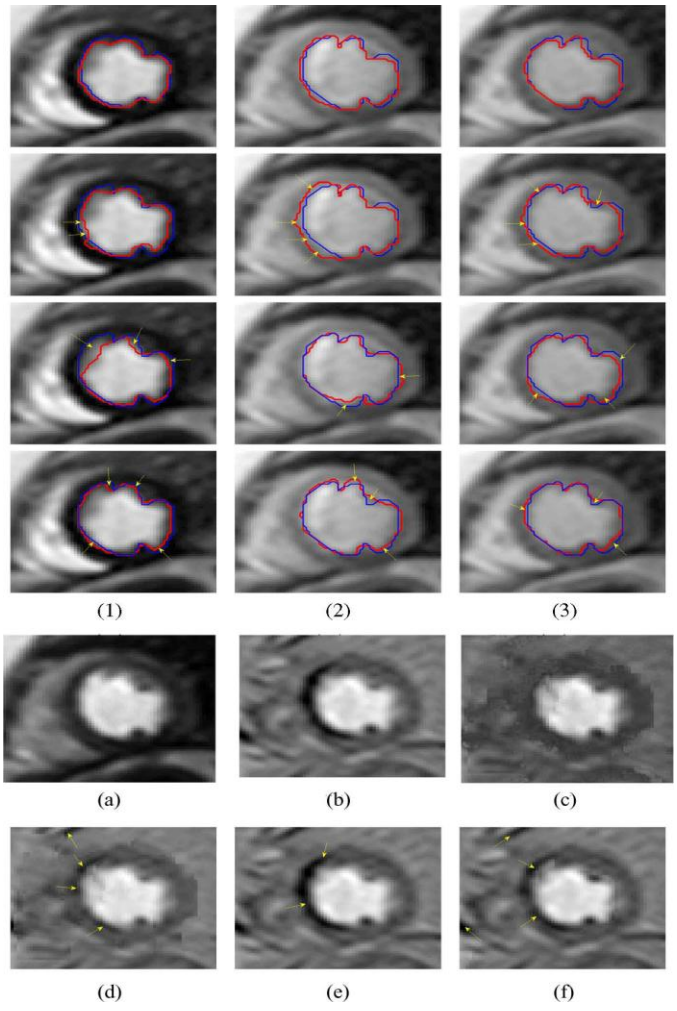

ISSN (Print) : 2320 – 3765
ISSN (Online): 2278 – 8875

International Journal of Advanced Research in Electrical, Electronics and Instrumentation Engineering

(An ISO 3297: 2007 Certified Organization)

Vol. 4, Issue 1, January 2015

Fig.3. Results for registration of cardiac images. Boundary of the LV (from *If*) deformed using the obtained motion field (in red) is overlaid on floating image. Blue contour is the outline of the LV in the reference image, shown in (a). First row shows results for *GSI*, second row shows results for *GI*, third row shows results for *Int*, and fourth row shows results for *Sal*. Columns (1)–(3) indicate floating images corresponding to different stages of contrast enhancement. Each column corresponds to the same floating image. (a)–(f) show difference images corresponding to the floating image in column (3): (a) reference image; (b) difference image before registration; difference after registration using (c) *GSI*; (d) *GI*; (e) *Int*; and (f) *Sal*. For the superimposed contours and difference images areas of misregistration using *GI*, *Int* and *Sal* are highlighted using yellow arrows.

However, by the combination of saliency and gradient information, *GSI* corrects these defects. The improvement in registration error (from Table I) is crucial for applications where correct diagnosis needs very accurate registration. Fig. 3(a)–(f) shows results based on difference images. The reference image is shown in Fig. 3(a), while the floating image is shown in Column (3). The difference image before registration is shown in Fig. 3(b). Fig. 3(c)–(f) shows, respectively, the difference images obtained after registration using *GSI*, *GI*, *Int*, and *Sal*.

As expected, *GSI* demonstrates the best registration accuracy. The regions of inaccurate registration in all images using the other three metrics are indicated by yellow arrows. Quantitative performance measures are shown in Table I for four scenarios, i.e., 1) Pre–Pre where the reference and floating images are both from the pre contrast stage; 2) Pre–Post where the reference image is from post contrast stage and the floating image is from pre contrast stage, or vice versa; 3) Post–Post where the reference and floating images are both from the post contrast stage; and 4) *Overall* which gives results for registering an entire image sequence comprising of pre- and post contrast images, and we choose one reference image that shows all tissues and organs clearly.

The values are for three evaluation criteria (NMI, *WC*, and Err) and five similarity metrics (*Int*, *Sal*, *GI*, *GSI*, and *FFD*). After accurate registration, NMI increases while *WC* and Err decrease compared to values before registration. Using intensity information does not show a significant improvement in results which indicates its limitations for registering perfusion images. For the other metrics, we observe improvement in registration with *GSI* showing the best results. The average error for the 12 datasets before registration varied from 2.1 to 4.5 mm indicating different degrees of motion and deformation. For accurate registration, the registered images are expected to have maximum error values of 1.2 mm. After registration using *GI*, the average Err varied from 1.2 to 1.8 mm with a maximum error of 2.8 mm. The average Err for *GSI* was between 0.7 and 1.2 mm with a maximum error of 1.8 mm. The maximum Err values for *Int* was 3.1 mm with the average ranging from 2.4 to 2.7 mm. For *Sal*, the maximum error was 2.4 mm and the average values were in the range 1.6–2.1 mm, while for *FFD* the maximum error was 1.9 mm with average values ranging from 1.2 to 1.7. For *GSI*, the average error after registration was less than 1 mm per pixel in 9 out of 12 datasets, while only four datasets had average error less than 1 mm for *GI* and *FFD*. Average Err for all datasets is shown in Fig. 2. The minimum and maximum errors were the least for *GSI*. After registration *WC* and Err decrease while *NMI* increases.

The calculation of Err was based on contours drawn manually by six clinical experts. The value of μ manual (see Section III-E) was 0.6. The small value of μ manual is a reflection of the consistency of the manually drawn contours. Greater consistency is observed between the manual contours for frames after contrast enhancement. From Table I, we observe that the improvement in Err between *Int* and all other methods is quite high. This clearly indicates the advantages of saliency and gradient information over intensity. The improvement in Err between *GI* and *GSI* is greater than μ manual. This indicates a significant improvement in performance due to *GSI* and makes the combination of saliency and gradient information a useful metric. *FFD*'s performance is similar to that of *GI*.

B. Effect of Saliency-Based Narrow Band Graph Cuts

We conduct a simple experiment to assess the effect of SNBGC on registration accuracy and speed. Elastic deformations on cardiac images were simulated using *FFD*s and then registered using our saliency-based method. In one set of experiments, we used a normal graph cut approach with different stages of coarse and fine optimization. In another set of experiments we used our SNBGC for coarse and fine optimization. Experiments on 20 images, with each having a different simulated deformation field, show that while the average error from conventional graph cuts (0.8 ± 0.2 mm) was almost the same as SNBGC (0.8 ± 0.3 mm), the computation times were significantly different (25.4 s for

ISSN (Print) : 2320 – 3765
ISSN (Online): 2278 – 8875

International Journal of Advanced Research in Electrical, Electronics and Instrumentation Engineering

(An ISO 3297: 2007 Certified Organization)

Vol. 4, Issue 1, January 2015

graph cuts and 4.1 s for SNBGC). Although the increase in average registration error for SNBGC is very less, the remarkable reduction in computation time definitely highlights the role of saliency in speeding up registration by identifying important pixels.

V. CONCLUSION

We have presented an MRF framework that combines saliency and gradient information for non rigid registration of contrast enhanced cardiac and liver images. Saliency was used in an attempt to imitate the working of the HVS which has a remarkable ability to match images in the presence of noise and contrast enhancement. We propose a modified saliency model based on neurobiological studies that are able to capture local changes in an image. This makes it suitable for elastic registration where matching local information is crucial. This model is different from the original model proposed in [19] that gave a global saliency map. Experimental results show that a combination of saliency and gradient information outperforms three other similarity metrics based on intensity, saliency, and gradient information. Although saliency provides highly similar maps for a pair of contrast enhanced images, its robustness can be further improved when used as a similarity measure. On the other hand, gradient information can be influenced by noisy datasets and does not accurately register the boundary of the LV in cardiac images. A combination of saliency and gradient information overcomes their individual limitations resulting in good registration performance. A saliency-based narrow band graph cut method was used to speed up the registration process. Saliency information was used to identify pixels undergoing deformations and reduce the number of graph nodes. Compared to conventional graph cuts, SNBGC showed a significant reduction in computation time and similar registration error. Experiments were conducted on real patient datasets showing elastic deformations. Compared to using only intensity, saliency and gradient information, a combination of saliency and gradient information shows considerable improvement in registration accuracy in terms of average registration errors.

REFERENCES

[1] T. Tang and C. Chung, "Nonrigid image registration using graph-cuts," in *Proc. Med. Image Comput. Comput.-Assist. Intervent. (MICCAI)*, 2007, pp. 916–924. [2] M. Holden, "A review of geometric transformations for nonrigid body registration," *IEEE Trans. Med. Imag.*, vol. 27, no. 1, pp. 111–128, Jan. 2008.
[3] R. Bajcsy and S. Kovacic, "Multiresolution elastic matching," *Comput. Vision. Graph.*, vol. 46, pp. 1–21, 1989.
[4] G. Christensen, M. Miller, and M. Vannier, "3-D brain mapping using a deformable anatomy," *Phys. Med. Biol.*, vol. 39, pp. 609–618, 1994.
[5] M. Bro-Nielsen and C. Gramkow, "Fast fluid registration of medical images," in *Proc. Vis. Biomed. Comput. (VBC)*, 1996, pp. 267–276.
[6] J.-P. Thirion, "Image matching as a diffusion process: an analogy with Maxwell's demons," *Med. Image Anal.*, vol. 2, pp. 243–260, 1998.
[7] C. Meyer, J. Boes, B. Kim, P. Bland, K. Zasadny, P. Kison, K. Koral, K. Frey, and R.Wahl, "Demonstration of accuracy and clinical versatility of mutual information for automatic multimodality image fusion using affine and thin-plate spline warped geometric deformations," *Med. Image Anal.*, vol. 1, pp. 195–206, 1997.
[8] D. Rueckert, L. I. Sonoda, C. Hayes, D. L. G. Hill, M. O. Leach, and D. J. Hawkes, "Nonrigid registration using free-form deformations: application to breast MR images," *IEEE Trans. Med. Imag.*, vol. 18, no. 8, pp. 712–721, Aug. 1999.
[9] Y. Zheng, J. Yu, C. Kambhamettu, S. Englander, M. Schnall, and D. Shen, "De-enhancing the dynamic contrast-enhanced breastMRI for robust registration," in *Proc. Med. Image Comput. Comput.-Assist. Intervent. (MICCAI)*, 2007, pp. 933–941.
[10] G. Rohde, A. Aldroubi, and B. Dawant, "The adaptive bases algorithm for intensity based nonrigid image registration," *IEEE Trans.Med. Imag.*, vol. 22, no. 11, pp. 1470–1479, Nov. 2003.
[11] C. Meyer, J. Boes, B. Kim, and P. Bland, "Probabilistic brain atlas construction: thin plate spline warping via maximization of mutual information," in *Proc. Med. Image Comput. Comput.-Assist. Intervent. (MICCAI)*, 1999, pp. 631–637.
[12] A. Shekhovtsov, I. Kovtun, and V. Hlav´ac, "Efficient MRF deformation model for non-rigid image matching," *Comput.Vision Image Understand.*, vol. 112, no. 1, pp. 91–99, 2008.
[13] B. Glocker, N.Komodakis, G. Tziritas,N.Navab, and N. Paragios, "Dense image registration through MRFs and efficient linear programming," *Med. Image Anal.*, vol. 12, no. 6, pp. 731–741, 2008.
[14] D. Mahapatra and Y. Sun, "Nonrigid registration of dynamic renal MR images using a saliency basedMRF model," in *Proc.Med. Image Comput. Comput.-Assist. Intervent. (MICCAI)*, 2008, pp. 771–779.
[15] W. Crum, T. Hartkens, and D. Hill, "Non-rigid image registration: Theory and practice," *Brit. J. Radiol.*, vol. 77, pp. 140–153, 2004.
[13] B Karthik, TVUK Kumar, Noise Removal Using Mixtures of Projected Gaussian Scale Mixtures, World Applied Sciences Journal, 29(8), pp 1039-1045, 2014.
[14] Daimiwal, Nivedita; Sundhararajan, M; Shriram, Revati; , Non Invasive FNIR and FMRI system for Brain Mapping .
[15] Daimiwal, Nivedita; Sundhararajan, M; , Functional MRI Study for Eye Blinking and Finger Tapping.
[16] Shriram, Revati; Sundhararajan, M; Daimiwal, Nivedita; , Effect of change in intensity of infrared LED on a photoplethysmogramIEEE Communications and Signal Processing (ICCSP), 2014 International Conference on, PP 1064-1067,2014.
[17] Kanniga, E; Srikanth, SMK; Sundhararajan, M; , Optimization Solution of Equal Dimension Boxes in Container Loading Problem using a Permutation Block AlgorithmIndian Journal of Science and Technology, V-7, I-S5,PP 22-26, 2014.
[21]Muralibabu, K; Sundhararajan, M; , PAPR performance improvement in OFDM system using DCT based on adjacent symbol groupingTrans Tech Publ, Applied Mechanics and Materials, V-550,PP 204-209, 2014